Exciton (De)Localization in the LH2 Antenna of *Rhodobacter sphaeroides* As Revealed by Relative Difference Absorption Measurements of the LH2 Antenna and the B820 Subunit

Vladimir Novoderezhkin,[†] René Monshouwer,[‡] and Rienk van Grondelle*[,‡]

A. N. Belozersky Institute of Physico-Chemical Biology, Moscow State University, Moscow 119899, Russia, and Department of Biophysics, Faculty of Sciences, Vrije Universiteit, De Boelelaan 1081, 1081 HV Amsterdam, The Netherlands

Received: November 17, 1998

We report the results of relative difference absorption measurements for the LH2 antenna of *Rhodobacter sphaeroides* and the B820 subunit of *Rhodospirillum rubrum* at room temperature. It is shown that significant differences between shapes and amplitudes of photoinduced, absorption changes reflect a different degree of exciton delocalization in the intact antenna compared with the dimeric subunit. Using the exciton model in the presence of static disorder, we have obtained a consistent and quantitative fit of the amplitudes and shapes of the pump−probe spectra of the LH2 antenna and the B820 subunit. We estimate that the nearest-neighbors interaction energy in the antenna is about 400 cm^{-1} and the diagonal disorder is about 450 cm^{-1}. For these values the coherence length (FWHM) of the steady-state exciton wavepacket corresponds to 5 BChl molecules at room temperature. The amplitude of the difference absorption reflects a cooperative behavior within at least 12 BChls of the B850 antenna. The calculations suggest that the dimeric subunit is characterized by a decrease of the interaction energy to 300 cm^{-1} together with an increase of the disorder value to about 600 cm^{-1}.

1. Introduction

The primary processes of photosynthesis include the absorption of light and excitation energy transfer in the light-harvesting antenna complexes with subsequent excitation trapping by the reaction center where a charge separation is initiated.[1] The light-harvesting antenna of purple bacteria generally consists of a peripheral antenna (LH2) and core antenna complexes (LH1), the latter directly surround the reaction centers. The elementary subunit of these complexes consists of a pair of transmembrane polypeptides, α and β, binding two or three bacteriochlorophyll (BChl) molecules.[2]

A high-resolution three-dimensional X-ray structure of the peripheral LH2 antenna was obtained for the purple bacteria *Rhodopseudomonas (Rps.) acidophila*[3] and *Rhodospirillum (Rs.) molischianum*.[4] It was shown that these antenna complexes consist of $\alpha\beta$ pigment−protein subunits arranged in a high-symmetry ringlike structure. For example, the LH2 antenna from *Rps. acidophila* contains 9 $\alpha\beta$ subunits, with each subunit binding two BChl850 molecules and one BChl800 molecule. Analysis of the pigment arrangement has shown that the 18 BChl850 molecules form a C_9-symmetry ring with a dimeric unit cell, whereas the 9 BChl800 molecules form a C_9-symmetry ring with a monomeric unit cell in a plane that is vertically displaced and parallel to the B850 ring. The Mg−Mg distance between the BChl850 pigments bound to the same $\alpha\beta$-polypeptide unit is 0.87 nm, and that between BChl850 pigments from neighboring dimeric units is 0.97 nm. The distances between nearest BChl800 molecules and between nearest BChl800 and BChl850 molecules are larger (2.1 nm and 1.8 nm, respectively). The structure of the LH2 antenna of *Rs. molischianum* is similar to that of *Rps. acidophila*, but this antenna complex consists of 8 $\alpha\beta$ subunits and the pigment−protein complex exhibits C_8-symmetery.

No high-resolution structure is available for the LH1 antenna, but analysis of 2D crystals of reconstituted LH1 from *Rhodospirillum (Rs.) rubrum* suggested that the core antenna is also arranged in a ring that consists of 16 $\alpha\beta$ subunits with each subunit binding two BChl875 molecules.[5]

These reports have stimulated new studies of the excitonic structure of these light-harvesting complexes[6−17] including experimental studies and theoretical simulations of the nonlinear optical response of the antenna.[17−35] However, the dynamics of electronic excitations in the antenna is still the subject of intensive debates. It is clear that the BChl arrangement in the form of a tightly-packed high-symmetry aggregate tends to delocalize electronic wavefunctions, but the intrinsic static and dynamic disorder of a pigment−protein complex may give rise to more localized states. The estimations of the degree of exciton delocalization gave values from 2 to 18 molecules for the B850 ring of the LH2 complex, i.e., from localization at one dimeric subunit to complete delocalization over the whole antenna (whole B850 ring). There are several reasons for such a large discrepancy.

First, the values of exciton coupling and the parameters of the disorder are not well-known. For example, the values of intradimer interaction energy were taken from 200 to 800 cm^{-1}, and the site inhomogeneity values (FWHM), from 200 to 700 cm^{-1} in the papers listed above. It is easy to calculate that different combinations of these two factors within such limits will give the delocalization size (the thermally averaged inverse participation ratio[32]) from 3 to 13 molecules for the B850 ring of the LH2 complex ($N = 18$) at room temperature.

Secondly, there are many different definitions of the delocalization degree that allow us to find different sizes of an

* To whom correspondence should be addressed.
[†] Moscow State University.
[‡] Vrije Universiteit.

10.1021/jp9844415 CCC: $18.00
Published on Web 11/06/1999

exciton for the same system. One group of definitions is dealing with individual exciton states. The delocalization of individual states can be obtained by calculating the squared wavefunction of the exciton states,[9] or the participation ratio for different eigenstates.[6,8,36] In the latter case the delocalization length can be defined as the inverse participation ratio. Typically, this value is different for different exciton eigenstates and it is convenient to introduce an effective delocalization length N_{eff} defined as the thermally averaged inverse participation ratio.[32] Another group of definitions deals with an exciton wavepacket, i.e., a superposition of exciton states. Such a superposition may exist due to coherent or noncoherent mixing of states under impulsive excitation of the antenna. The evolution of the wavepacket is described by the density matrix.[25,30−33,37] The coherence length (or delocalization length) of the wavepacket is characterized by the decay of the density matrix in the antidiagonal direction.[30−33] The coherence length N_{coh} can be defined as the FWHM of this antidiagonal distribution.[25] In the steady-state limit (for time delays longer than exciton relaxation) the N_{coh} value is determined by a superposition of exciton states that are populated at thermal equilibrium.

Using these definitions, we will obtain very different exciton sizes even in the case of the homogeneous antenna. In this case the wavefunctions are completely delocalized over the whole B850 ring, i.e., over 18 molecules. The lowest exciton level has a uniform wavefunction, the corresponding inverse participation ratio is equal to 18. For higher levels the wavefunctions are oscillating, resulting in nonequal participation of different molecules in these states, and giving rise to the inverse participation ratio of 12. The thermally averaged inverse participation ratio is $N_{eff} = 13-14$ at room temperature and for interaction energies corresponding to the middle of the 200−800 cm^{-1} range. For the same parameters the coherence length of the steady-state wavepacket is $N_{coh} = 6-7$. It means that even in the homogeneous (i.e., completely delocalized) case the effective exciton sizes as revealed by widely accepted definitions are significantly less than the size of a whole ring. If we switch on the disorder, these values will be even smaller. Thus, modeling of the LH1 and LH2 antennas with the presence of static disorder gave the values $N_{eff} = 5-11$[6,8,17,21,30] and $N_{coh} = 4-6$[17,21,25] at room temperature. In all these models the exciton−phonon coupling was supposed to be weak. In the weak coupling limit the steady-state coherence length does not depend on the nature of the phonons and the exciton−phonon coupling strength, being determined by the static disorder only.[32] The situation changes in the case of strong exciton−phonon coupling. The strong coupling may give rise to further reduction of the exciton size due to polaron formation.[32−35] It can be significant if the phonon-induced localization length (polaron size) will be smaller than the disorder-induced localization length.

Notice that both N_{eff} and N_{coh} values reflect a nonuniformity of the shape of the exciton wavefunction, but not any physical size. For example, if we cut off a fragment of the ring containing a number of molecules equal to N_{eff} or N_{coh}, we, in general, will not be able to reproduce all essential properties of the antenna, such as its spectral properties. Generally, a spectral response of a strongly coupled aggregate reflects a cooperative behavior of some number of pigments that can be very different from the effective localization sizes, N_{eff}, N_{coh}.[11,30,38] This number of molecules can also be different for different spectroscopic techniques. For example, the shape of the pump−probe spectra of the antenna is controlled by the so-called exciton mean-free path, which is less than the localization size N_{coh}.[30] On the other hand, the shape of the CD spectra of the B850 band of the LH2 antenna is determined by cooperativity within at least 10−12 molecules.[11,38] One could define the spectroscopic subunit as the minimal fragment of the ring that is big enough to reproduce all spectral features of the whole antenna.[38] Due to disorder, the size of such a subunit is less than the aggregate size N, but more than both effective localization sizes, N_{eff} and N_{coh}.

In this paper we study the exciton delocalization in the LH2 antenna of *Rhodobacter (Rb.) sphaeroides* using the relative difference absorption (pump−probe) measurements of the LH2 antenna and the B820 subunit. This technique allows us to quantitatively compare the spectral shapes and amplitudes of the nonlinear response of the whole antenna with those of the dimeric subunit. Generally, the spectrum of the dimeric subunit has a different shape, amplitude and red shift as compared with the whole antenna. These spectral differences were indeed observed by us, and they reflect a different degree of exciton delocalization in the antenna as compared with the dimeric subunit. Using this data, we can precisely estimate the delocalization parameters N_{eff} and N_{coh} and the size of the spectroscopic subunit.

It is clear that this method is more informative and more precise than the conventional pump−probe studies where so far only the shape of the pump−probe spectra of the antenna is detected and modeled. In fact, the fitting of such spectral shapes using a model with excitonic interactions and spectral disorder is not very sensitive to the choice of the interaction energies and the disorder values. For example, in the previous paper[17] we have obtained a simultaneous fit of the absorption and pump−probe spectra of the LH1 antenna using the interaction energy values from 260 to 600 cm^{-1} and the site inhomogeneity values from 400 to 500 cm^{-1}. The corresponding delocalization length N_{eff} was changing from 3.8 to 9.1 for these different fits. This means that we are not able to estimate the delocalization length from the shape of the pump−probe spectra only. On the other hand, we have also calculated the amplitude of the bleaching peak of the pump−probe spectra normalized to the bleaching of the BChl monomer[17] and we found that this relative bleaching value was varying from 5.4 to 11.2 in close correlation with the N_{eff} value. So, the amplitude of the difference absorption contains information that can be used for a more precise estimation of the delocalization parameters. Unfortunately, these bleaching amplitudes cannot be directly obtained from the pump−probe spectra. The only possibility is to compare the bleaching values of the antenna with those of some reference system.

In the case of B800-850 (LH2) complexes, it is possible to compare the bleaching values of the B850 ring to that of the B800 monomer.[19] Similarly, for the B808-866 complex from the green bacterium *Chloroflexus (Cf.) aurantiacus*, the bleaching value of the B866 band can be compared with that of the monomeric B808 band.[20,21] In the case of the core (LH1) antenna, it is possible to compare the amplitude of the difference absorption in the antenna with the bleaching of the BChl dimer (special pair) of the reaction center,[39,40] although these experiments are very sensitive to annihilation processes occurring upon multiphoton excitation of the antenna. In both cases the spectral parameters of the reference system are different from the parameters of the B850 (B866) ring or LH1 antenna. So, the comparison of the spectral shapes of these reference systems with those of the circular antenna aggregate yields no additional information about the relevant spectroscopic parameters of the antenna. Only the difference in the bleaching amplitudes is of

interest, reflecting the delocalized character of the exciton wavefunctions of the antenna.

In this paper we use the same idea of the relative difference absorption measurements, but here we take as a reference the building block of the antenna itself. This dimeric subunit should exhibit all the essential properties of the antenna: the pigment−pigment interaction energy, the static and dynamic disorder (line broadening) having the same origin, and most probably, the same (or close) values as for the whole antenna. It means that the only reason of any difference in amplitudes and shapes of the corresponding pump−probe spectra is the different delocalization degree for the antenna and for its subunit. So, not only a quantitative comparison of the amplitudes but also a comparative analysis of spectral shapes of the two systems is of great interest in this approach. The challenge is to explain all features (amplitude and shape) of the pump−probe spectrum of the dimeric subunit using the same physical model and the same parameters as those used in the fit of the pump−probe spectrum of the whole antenna.

2. Experimental Section

We have measured the difference absorption spectra of the LH2 antenna of *Rhodobacter (Rb.) sphaeroides* using as a calibration the difference absorption spectrum of the B820 subunit of *Rs. rubrum*. LH2 and B820 were prepared as described in ref 41. The difference absorption measurements were done using a laser system described in refs 41 and 42. The pump wavelength was selected from the white light continuum using a narrow bandpass filter at 830 nm. Pump and probe pulse duration was 150 fs. We have used the same outside diameter (o.d.) at the excitation wavelength for both samples (about 0.3 per 2 mm). To correct for annihilation in the LH2 sample, we have measured the intensity dependence of the difference absorption signals of this sample. Annihilation in the LH2 complex was present for the range of excitation densities used (5−57 nJ). To extrapolate the measured intensity dependence to the amplitude expected in the absence of annihilation, we have used the intensity dependence in the Poisson saturation limit.[41] The extrapolated value was used to correct the amplitude of the LH2 spectrum. This amplitude was then normalized to the number of absorbed photons. The B820 spectrum was measured using an excitation density of 30 nJ. Since no transfer takes place, there is no annihilation and the spectrum can be directly normalized to the number of absorbed photons. All measurements were performed at room temperature.

3. Model of the Bacterial Light-Harvesting Antenna

In the model for LH2 we suppose that the pigment organization of the LH2 antenna of *Rb. sphaeroides* is analogous to that of the LH2 antenna from *Rps. acidophila*. The B850 inner circle consists of 18 BChl *a*, which form a ring with C_9-symmetry (the elementary unit cell contains two BChl850 molecules, bound to the α and β polypeptides). The Q_y transition dipole moments of the two BChls in a dimeric unit cell have the angles ψ_1 and ψ_2 with the plane of the circle and angles φ_1 and φ_2 with the tangent to the circle. The energies of the electronic transition of these two BChls are E_1 and E_2. The difference between these energies, $\Delta E = E_1 - E_2$, was varied from 0 to 500 cm^{-1}. The ratio of transition dipoles for the S_1-S_2 and S_0-S_1 transitions in the BChl monomer, χ, was varied from 0 to 1.5. The Mg−Mg distance between BChls in a dimeric unit is r_{12} and between nearest BChls from neighboring units is r_{23}. We supposed that $\psi_1 = 10°$, $\psi_2 = 5°$, $\varphi_1 = 20°$, $\varphi = 200°$, $r_{12} = 0.87$ nm, and $r_{23} = 0.97$ nm (these parameters are approximately the same as those for the B850 circle of the LH2 antenna from *Rps. acidophila*).[3] In our simulations of the B850 absorption band we have taken into account the interactions between the Q_y transitions of BChls, neglecting their mixing with Q_x, B_y, B_x transitions as well as with charge transfer states.[8]

We supposed that the interaction energies between the BChl molecules are $M_{12} = 400$ cm^{-1}, $M_{23} = 290$ cm^{-1}, $M_{13} = -52$ cm^{-1}, and $M_{14} = 14$ cm^{-1}, where M_{12} corresponds to the intradimer interactions, M_{23} to interdimer nearest-neighboring interactions, M_{13} to second neighbors interactions, and M_{14} to third neighbors interactions. We also performed calculations using alternative choices for the interaction energies: $M_{12} = 300$ and 500 cm^{-1} instead of $M_{12} = 400$ cm^{-1}, with a corresponding scaling of M_{23}, M_{13}, and M_{14}. Note that microscopic calculations using the point charge approximation gave $M_{12} = 806$ cm^{-1}, $M_{23} = 377$ cm^{-1}, and $M_{13} = -152$ cm^{-1} for the LH2 complex of *Rs. molischianum*[10] and $M_{12} = 197-545$ cm^{-1} and $M_{23} = 158-461$ cm^{-1}, with various treatment of the dielectric screening, for the LH2 complex of *Rps. acidophila*.[8] A recent *ab initio* calculation gave $M_{12} = 320$ cm^{-1} and $M_{23} = 255$ cm^{-1} for the LH2 complex of *Rps. acidophila*.[16] For the LH2 complex of *Rb. sphaeroides* an analysis of the CD spectrum yielded $M_{12} = 300$ cm^{-1} and $M_{23} = 233$ cm^{-1}.[12]

The B820 subunit is the $\alpha\beta BChl_2$ building block of LH1[43−45] and has been shown to be best described as a "disordered dimer" of BChls, for which the excitonic interaction was estimated to be 230 cm^{-1}.[45−48] We have used two different models for the B820 subunit. In the first model we suppose that the structure of this subunit as well as other parameters (exciton coupling, site inhomogeneity, homogeneous line widths) is the same as for a dimeric unit within the LH2 antenna. This is not completely true because this subunit is in fact extracted from the LH1 antenna, and the parameters of the $\alpha\beta BChl_2$ building block of LH1 and LH2 may be different. Additional changes may arise due to extraction of a dimeric subunit from the antenna. That is why we also considered an alternative model of the B820 subunit for which the main parameters are slightly different from those of the antenna.

The site inhomogeneity of the antenna was described by a normal distribution of uncorrelated perturbations to the electronic energies of the BChl pigments. The width (FWHM) of this distribution, σ, was varied from 0 to 1000 cm^{-1}. The Monte-Carlo calculations of the pump−probe spectra include the following.

(1) Direct numerical diagonalization of the one- and two-exciton Hamiltonian for 1000-4000 realizations of the diagonal energies. We used the standard Hamiltonian for a Frenkel exciton in the Heitler−London approximation.[49] The corresponding explicit form of the one- and two-exciton Hamiltonian for an aggregate of three-level molecules is given in ref 25. The exciton−phonon interactions were not taken into account.

(2) Calculation of homogeneously broadened spectra from stick spectra (for each set of diagonal energies). We assumed Gaussian line shapes with homogeneous line widths (FWHM) Γ_{1L}, Γ_{1H}, Γ_{2L}, Γ_{2H}, corresponding to transitions from the ground state to the lowest one-exciton level (Γ_{1L}), from the ground state to higher one-exciton levels (Γ_{1H}), from the lowest one-exciton level to two-exciton levels (Γ_{2L}), and from higher one-exciton levels to two-exciton levels (Γ_{2H}). The Stokes shift of the stimulated emission is S. The parameters Γ_{1L}, Γ_{1H}, Γ_{2L}, Γ_{2H}, and S are variables and should be determined from a fit of the experimental data.

(3) Averaging of the homogeneously broadened spectra over a random distribution of diagonal energies (convolution of homogeneous and inhomogeneous line shapes).

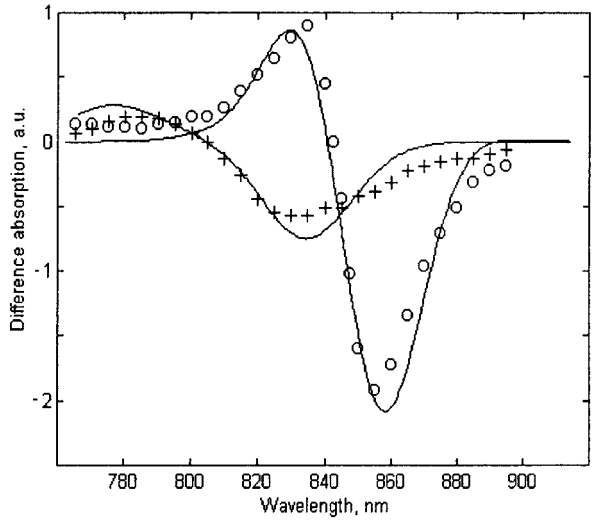

Figure 1. Simultaneous fit of experimental pump−probe spectra for the B850 band of the LH2 antenna from *Rb. sphaeroides* (circles) and for the B820 subunit from *Rs. rubrum* (pluses) at room temperature. The delay between the pump and probe is 10 ps. The excitation wavelength is 830 nm, and the excitation density is 30 nJ. Both spectra are normalized to the number of absorbed photons. Calculated curves for $N = 18$ and $N = 2$ are shown by solid lines. The interaction energies are $M_{12} = 400$ cm^{-1}, $M_{23} = 290$ cm^{-1}, $M_{13} = -52$ cm^{-1}, and $M_{14} = 14$ cm^{-1}. Line widths: $\Gamma_{1L} = 280$ cm^{-1}, $\Gamma_{1H} = 360$ cm^{-1}, $\Gamma_{2L} = 430$ cm^{-1}, $\Gamma_{2H} = 470$ cm^{-1}. The Stokes shift is $S = 130$ cm^{-1}, and the site inhomogeneity is $\sigma = 450$ cm^{-1}.

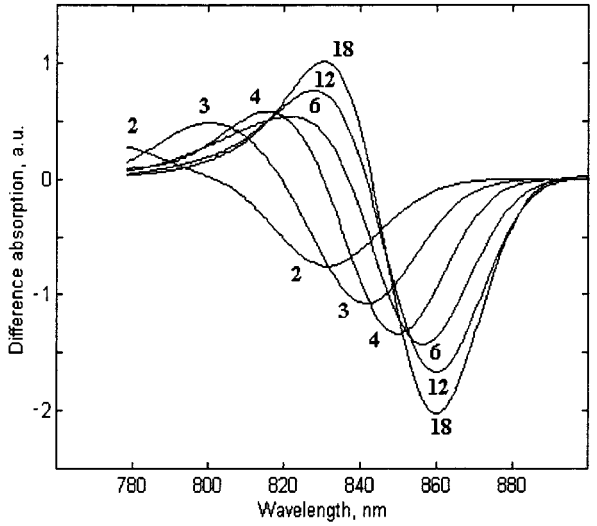

Figure 2. Pump−probe spectra calculated for the whole B850 ring ($N = 18$) and for a fragment of the ring containing N molecules ($N = 2$, 3, 4, 6, 12). The interaction energies, site inhomogeneity, and line widths for the fragment are the same as for the whole ring (the same as in Figure 1).

We have calculated the pump−probe spectra for the whole B850 ring as well as for an arbitrary part of the ring. In the latter case we supposed that some fragment containing N molecules ($N < 18$) was cut out and extracted from the antenna. For example $N = 2$ corresponds to the dimeric subunit (with intermolecular distance r_{12} and interaction energy M_{12}), the $N = 3$ fragment contains three molecules (intermolecular distances are r_{12} and r_{23}, the interaction energies are M_{12} and M_{23}). $N = 4$, 6, and 12 correspond to two, three, and six dimeric subunits, and $N = 18$ corresponds to the whole ring. We have assumed that the parameters Γ_{1L}, Γ_{1H}, Γ_{2L}, Γ_{2H}, S, σ, χ, and ΔE are the same for all the fragments, i.e., independent of N.

4. Results

Shape and Amplitude of Difference Absorption Spectrum. The measured and calculated pump−probe spectra are shown in Figure 1. Experimental spectra were obtained for the B850 band of the LH2 antenna from *Rb. sphaeroides* and for the B820 subunit from *Rs. rubrum* at room temperature. The delay between pump and probe pulses was 10 ps corresponding to the steady-state limit (with respect to excitonic and vibrational relaxation). The LH2 spectrum was corrected for annihilation effects as discussed in the experimental section and normalized to the number of absorbed photons per one B850 antenna ($N = 18$). The B820 spectrum was annihilation free and normalized to the number of absorbed photons per one subunit ($N = 2$). The calculated data correspond to the simultaneous fit for the B850 antenna and the B820 subunit; i.e., all parameters of the B820 subunit (M_{12}, Γ_{1L}, Γ_{1H}, Γ_{2L}, Γ_{2H}, S, σ, χ, and ΔE) are the same as for the B850 antenna. A best fit was obtained for $\Gamma_{1L} = 280$ cm^{-1}, $\Gamma_{1H} = 360$ cm^{-1}, $\Gamma_{2L} = 430$ cm^{-1}, $\Gamma_{2H} = 470$ cm^{-1}, $S = 130$ cm^{-1}, $\sigma = 450$ cm^{-1}, $\chi = 0.3$, and $\Delta E = 0$. Variation of ΔE between 0 and 200 cm^{-1} does not influence the shapes of both spectra, but when ΔE becomes comparable with the interaction energy, M_{12}, it increases the splitting between the positive and negative peaks of the pump−probe spectrum of the dimeric subunit (without significant changes in the spectrum of the B850 antenna). The shapes and amplitudes of the experimental spectra are satisfactorily reproduced with $\chi < 0.3$, but for larger χ values, this becomes increasingly more difficult (especially for the dimeric subunit). All other parameters were determined from the fit with an accuracy of about 5%. The monomeric transition energy was used as a free parameter to obtain the true position of the bleaching peak of the LH2 antenna, but once its value was established it was not changed (as well as the values of the other parameters) when the dimeric subunit spectrum was calculated. It can be concluded from Figure 1 that we have obtained a simultaneous and reasonable fit of both experimental spectra, within the context of the model outlined above. In this model all parameters are the same for the two systems, the ringlike B850 antenna and the B820 dimeric subunit. The only difference is in the boundary conditions. To model the spectrum of the subunit, we just simply switched off all the interactions outside one fixed dimer of the antenna. This is enough to reproduce the changes in the shape of the pump−probe spectrum and its blue shift together with the 3-fold decrease in bleaching amplitude. Notice, however, that the experimental spectra are more asymmetric than the calculated ones. This asymmetry is most probably due to the presence of vibrational and/or phonon sidebands, which contribute to the red wings of the stimulated emission borrowing some part of the dipole strength from shorter wavelengths.

To study in more detail the relation between the size of the aggregate and its spectral features, such as the shape, amplitude, and red shift of the difference absorption, we have calculated pump−probe spectra for $N = 2$, 3, 4, 6, 12, and 18 (Figure 2). All parameters are the same as those in Figure 1.

In the small aggregate limit ($N = 2$, 3, 4) the amplitude of the bleaching peak increases proportional to N, but for larger N the rate of this increase becomes much slower (compare the bleaching values for $N = 6$, 12, 18). This is explained by the following simple argument. Within the framework of the exciton model discussed above, the shape of the difference absorption spectrum is determined by the negative component due to photobleaching (PB) and stimulated emission (SE) of one-exciton states, and by the positive component due to excited state absorption (ESA) from one-exciton to two-exciton states.

The most intense ESA lines correspond to transitions from a few of the lower one-exciton levels to the lowest two-exciton states and are blue shifted with respect to the PB/SE lines. This gives rise to the specific sigmoid shape of the spectrum, which is typical for the circular aggregate and for the open quasi-linear chain.[50,51] In small aggregates the one-exciton and the two-exciton contributions (PB/SE and ESA) are well separated spectrally; i.e., the splitting between the most intense PB/SE and ESA lines is larger than the corresponding line widths. In this case the third-order nonlinear susceptibility increases proportionally to N^2, so that the amplitude of the bleaching peak normalized to the number of absorbed photons (per one aggregate) increases proportional to N. An increase in aggregate size, N, reduces the exciton splitting and increases the overlap of the PB/SE and ESA components. The nonlinear susceptibility has two contributions, both of order N^2, but due to their overlap the resulting susceptibility increases proportional to $(c_1N - c_2)$, where c_1 and c_2 are some constants. The normalized amplitude of the bleaching peak is proportional to $(c_1 - c_2/N)$. The crossover size, N_C, where the scaling of the nonlinear response changes from N^2 to N is equal to[37]

$$N_C = \pi(2M/\Gamma)^{1/2} \quad (1)$$

where M is the interaction energy and Γ is the line width of the excitonic transitions. Taking $M = 400$ cm^{-1} and $\Gamma = 300-400$ cm^{-1}, we obtain $N_C = 4.44-5.13$, i.e., $N_C = 5$.

The red shift of the lowest exciton level of the quasilinear aggregate is $2M\cos(\pi/(N+1))$, varying from M to $1.73M$ in the small aggregate limit ($N \leq N_C$), and from $1.8M$ to $2M$ for the larger aggregates ($N > N_C$). This explains the result of Figure 2 where we obtained a linear increase of the difference absorption amplitude together with increasing of the red shift for $N = 2$, 3, and 4 and a much slower increase of the amplitude with approximately constant red shift for $N = 6$, 12, and 18.

Alternative Choice of Interaction Energies. We also performed calculations using alternative choices for the interaction energies: $M_{12} = 300$ and 500 cm^{-1} instead of $M_{12} = 400$ cm^{-1}, used in Figure 1. For both these alterations of M_{12} we performed a corresponding scaling of M_{23}, M_{13}, and M_{14}. Taking these interaction energies, it was possible to reproduce the ratio of the bleaching amplitudes of the LH2 antenna and the B820 dimeric subunit using approximately the same σ/M_{12} value, i.e., taking $\sigma = 340$ and 550 cm^{-1} for $M_{12} = 300$ and 500 cm^{-1}, respectively. But in this case the position of the bleaching peak of the B820 subunit cannot be explained if we use the same monomeric energy for B820 as for the LH2 antenna. That is why the monomeric transition for the dimeric subunit should be shifted with respect to that of LH2 antenna by 7 nm to the blue for $M_{12} = 300$ cm^{-1} and by 10 nm to the red for $M_{12} = 500$ cm^{-1}. Furthermore, for both cases the fit to the experimental spectra is not as good as for $\sigma = 450$ cm^{-1} and $M_{12} = 400$ cm^{-1} (data not shown). Variation of the line width values does not improve these results.

Independent Fit of the Two Difference Spectra. So far in our fitting of the difference spectra, we supposed that the B820 dimeric subunit has exactly the same structural and spectroscopic parameters as the BChl dimer in the LH2 antenna. This assumption allowed us to obtain a reasonable fit of the experimental data (see Figure 1). This fit may be improved if we suppose that the parameters of the B820 subunit are somewhat different from those of the B850 antenna (due to structural differences of the LH1 and LH2 complexes and/or due to the extraction procedure). For example, we can better explain the splitting between the ESA and PB/SE components of the B820 spectrum if we assume that in B820 the intradimer interaction energy has decreased slightly. A better fit of the shape of this spectrum can be obtained if we further suppose that the site inhomogeneity value has increased.

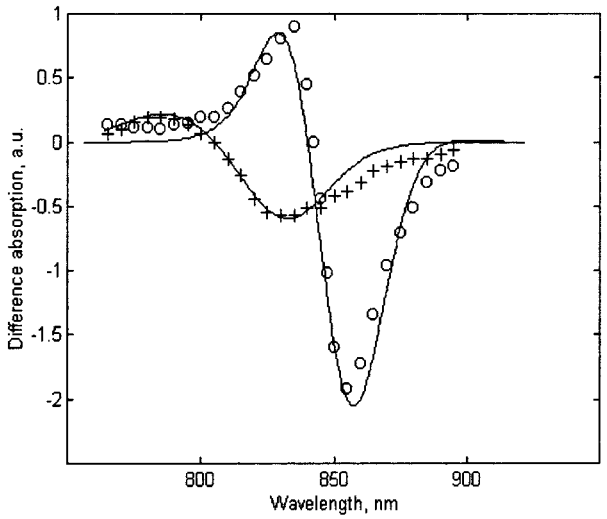

Figure 3. Independent fit of pump−probe spectra of the LH2 antenna and of the B820 subunit. Parameters for the antenna: $M_{12} = 400$ cm^{-1}, $\sigma = 450$ cm^{-1}, $\Gamma_{1L} = 240$ cm^{-1}, $\Gamma_{1H} = 340$ cm^{-1}, $\Gamma_{2L} = 400$ cm^{-1}, $\Gamma_{2H} = 440$ cm^{-1}, $S = 130$ cm^{-1}. Parameters for the B820 subunit: $M_{12} = 300$ cm^{-1}, $\sigma = 600$ cm^{-1}, $\Gamma_{1L} = 280$ cm^{-1}, $\Gamma_{1H} = 360$ cm^{-1}, $\Gamma_{2L} = 460$ cm^{-1}, $S = 130$ cm^{-1}. The monomeric transition for the dimeric subunit was 8 nm red shifted with respect to that of the antenna. Experimental data: the same as in Figure 1.

The result of the independent fit of the pump−probe spectra of the LH2 antenna and of the B820 subunit is shown in Figure 3. We have used the following parameters for the antenna: $M_{12} = 400$ cm^{-1}, $\sigma = 450$ cm^{-1}, $\Gamma_{1L} = 240$ cm^{-1}, $\Gamma_{1H} = 340$ cm^{-1}, $\Gamma_{2L} = 400$ cm^{-1}, $\Gamma_{2H} = 440$ cm^{-1}, $S = 130$ cm^{-1}. The parameters for the B820 subunit are $M_{12} = 300$ cm^{-1}, $\sigma = 600$ cm^{-1}, $\Gamma_{1L} = 280$ cm^{-1}, $\Gamma_{1H} = 360$ cm^{-1}, $\Gamma_{2L} = 460$ cm^{-1}, and $S = 130$ cm^{-1}. The B820 subunit in this model is characterized by a decrease in exciton coupling and an increase in the site inhomogeneity and the homogeneous line widths. The monomeric transition for the dimeric subunit was 8 nm red shifted with respect to that of the LH2 antenna. This independent fit of the pump−probe spectra is clearly better than the simultaneous fit of the LH2 antenna and B820 subunit (compare Figures 3 and 1). Using the same parameters, we have also calculated the linear absorption. The FWHM of the LH2 and B820 absorption spectra are 29.5 and 35.7 nm, respectively. If we use the parameters from the simultaneous fit (the same as in Figure 1) we obtain 30.6 and 28.7 nm, respectively. For comparison, the experimental widths are 29 nm for the B850 band of LH2 of *Rb. sphaeroides*[52] and 38 nm for the B820 subunit from *Rs. rubrum* at room temperature.[53] These values are closer to the results of our independent fit.

In conclusion, a better fit of the linear absorption and pump−probe spectra can be obtained if we suppose that after the extraction procedure the dimeric subunit exhibits some structural rearrangement, leading to a slight decrease of the pigment−pigment interaction and an increase of the coupling with slow and/or fast protein motions. The latter gives rise to an increase in the amount of static and dynamic disorder (inhomogeneous and homogeneous broadening). The proposed structural rearrangement is further corroborated by a recent Stark spectroscopy study of the B820 subunit,[54] which showed that in contrast to LH1/2 the Stark signal of the B820 subunit is small, most likely due to a loss of charge transfer interactions between the two

BChls in the dimer as compared to the case of LH1/2 (for more details see discussion in ref 55). Our fitting in fact suggests that the intradimer interaction energy of B820, $M_{12} = 300$ cm^{-1}, is approximately the same as the estimated interaction between two BChls from adjacent dimers of the antenna, $M_{23} = 290$ cm^{-1}. Therefore, we may also suppose that B820 is not a rearranged dimeric subunit, but just two BChls from neighboring subunits that have a larger center-to-center distance and significantly lower overlap of the electron densities.[3] This could then implicate that the large Stark spectrum of LH1 arises from the "real" $\alpha\beta$BChl$_2$ dimer.

Notice that in the earlier studies of the B820 subunit by means of CD, polarized fluorescence, and singlet minus triplet spectroscopies,[45,46,53] the interaction energy within this subunit was estimated as $M = 230$ cm^{-1} and the site inhomogeneity as $2M$ at 77 K and $3M$ at room temperature, i.e., 460 and 690 cm^{-1}, respectively, in very reasonable agreement with our results.

Exciton Delocalization Degree. Quantitative information about the delocalization of the exciton wavefunctions can be obtained using the participation ratio defined as[36]

$$L_k = \sum_{n=1}^{N} |c_n^k|^4 \qquad \sum_{n=1}^{N} |c_n^k|^2 = 1 \tag{2}$$

where c_n^k is the amplitude of the kth eigenfunction corresponding to the nth site. The inverse participation ratio, $(L_k)^{-1}$ determines the delocalization length of kth exciton state. The thermally averaged inverse participation ratio is defined as[32]

$$N_{\text{eff}} = \langle Z^{-1} \sum_k (L_k)^{-1} \exp(-E_k/k_B T) \rangle$$

$$Z = \sum_k \exp(-E_k/k_B T) \tag{3}$$

where E_k is the energy of the kth one-exciton state, k_B is the Boltzmann constant, T is temperature, and brackets indicate an average over realizations of the disorder. The participation ratio for the states at energy E is described by the function[36]

$$L(E) = \langle \sum_k L_k \delta(E - E_k) \rangle / \langle \sum_k \delta(E - E_k) \rangle \tag{4}$$

The participation ratios $L(\lambda)$, where λ is wavelength corresponding to the energy E, are shown in Figure 4 for the B820 subunit and for the B850 antenna. In this calculation we replaced the δ-function in eq 4 by a Gaussian function with a FWHM of 3 cm^{-1}. All other parameters are the same as in Figure 1.

For the dimeric subunit the participation ratio is 0.52−0.55. This is very close to the homogeneous limit, i.e., 0.5, corresponding to complete delocalization over two molecules. The site inhomogeneity is less than the splitting between two exciton levels ($\sigma < 2M_{12}$) and cannot significantly destroy the zero-order (homogeneous) exciton wavefunction. If we use the site inhomogeneity and interaction energy for the dimeric subunit as in Figure 3 (i.e., $\sigma = 2M_{12}$), the participation ratio will be slightly higher: 0.56−0.61 (data not shown).

For the B850 antenna the participation ratio is 0.1 in the middle of the band, is about 0.13 close to the absorption maximum (850 nm), and increases to above 0.3 in the red wing. This implies that individual exciton states are highly delocalized in the middle of the band but are more localized in the red edge. For the lowest levels ($k = 0, \pm1, \pm2$) the inverse participation ratio, $(L_k)^{-1}$, averaged over disorder is equal to 5.8, 7.0, 8.9, 9.0, and 10.1 (in increasing order of energy). The thermally averaged inverse participation ratio is $N_{\text{eff}} = 7.87$ at room temperature. This is different from the homogeneous limit when the inverse participation ratio is 12 for the lowest level and 18 for the higher ones, and $N_{\text{eff}} = 13.4$ at room temperature. The difference originates from a mixing of the zero-order wavefunctions induced by the site inhomogeneity. The degree of mixing is higher than in the dimer because the splitting between the exciton levels in the LH2 antenna is much less, decreasing as $\sim N^{-1}$ in the middle and $\sim N^{-2}$ near the edges of the band.

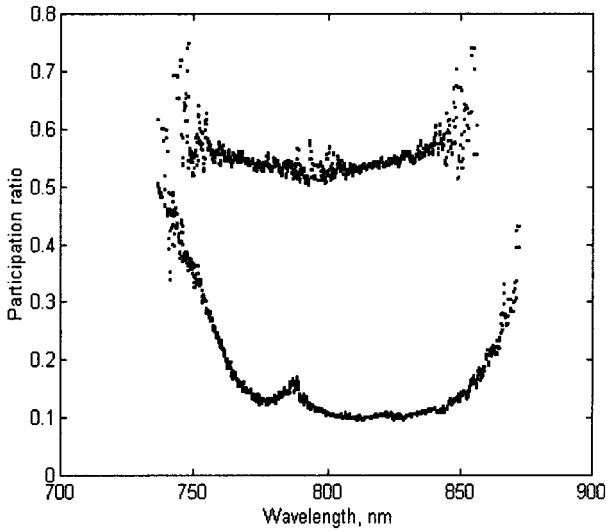

Figure 4. Participation ratio for the dimeric subunit (upper curve) and for the whole antenna (lower curve) calculated for the same parameters as in Figure 1.

We note that the inverse participation ratio corresponds to a delocalization length for individual exciton states only. However, in general we are always dealing with some kind of superposition of exciton levels. For zero time delay (immediately after excitation) such a superposition may exist due to coherent or noncoherent mixing of states under impulsive excitation of the antenna. In the steady-state limit (for time delays longer than exciton relaxation) we will have a superposition of exciton states that are populated at thermal equilibrium. In the case of the dimeric subunit, superposition of levels is negligible because the splitting between the two exciton levels, $2M_{12}$, is much larger than the spectral width of the pump pulse and also much larger than $k_B T$. In contrast, for the whole antenna we may expect an exciton wavepacket that is a superposition of several exciton levels.

Evolution of the initially formed exciton wavepacket in the antenna (or selectively excited single exciton state) to the steady-state wavepacket can be described by the one-exciton density matrix in the site representation, $\rho_{m,n}(t)$, where n and m are molecular numbers.[25,30,31] The decay of the density matrix elements in the antidiagonal direction is determined by delocalization length (or coherence length) of the exciton wavepacket.[30−32] In the literature there are different definitions for this length. Meier et al.[30] defined the coherent size, N_ρ, as the participation ratio of the density matrix. Kühn and Sundström[25] introduced the coherence function

$$C(n) = \sum_{m=1}^{N} |\langle \rho_{m,m+n} \rangle| \tag{5}$$

and defined the coherence length, N_{coh}, as the FWHM of the $C(n)$ distribution. Typically, N_{coh} is significantly less than N_ρ, as can be seen from the density matrix plot obtained by Meier et al.[30] For example, for the B850 band of the LH2 antenna

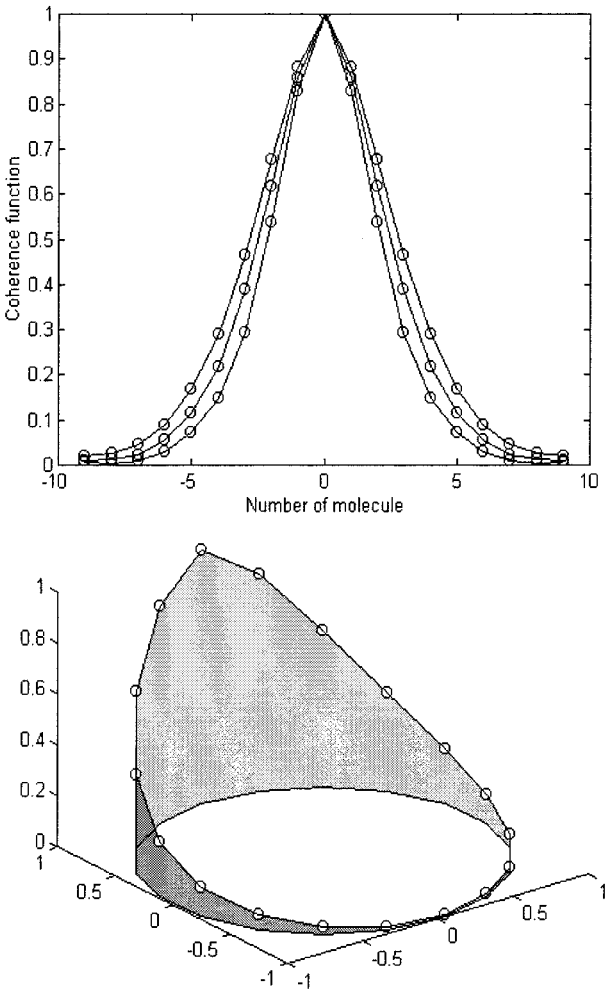

Figure 5. Steady-state coherence function for the LH2 antenna at room temperature with $M_{12} = 300$, 400, and 500 cm^{-1}. The lower interaction energy corresponds to a narrower coherence function; see the top frame. The site inhomogeneity values are $\sigma = 340$, 450, and 550 cm^{-1}, respectively. The effective coherence length (FWHM) is calculated to be $N_{coh} = 4.4$, 5.0, and 5.7 for the three interaction energies, respectively. Bottom frame: a three-dimensional view of the coherence function for $M_{12} = 400$ cm^{-1}. The *x*- and *y*-coordinates correspond to the positions of the BChl molecules in the plane of the ring.

$N_{coh} = 8$, $N_\rho = 15$ at 4.2 K and $N_{coh} = 5$, $N_\rho = 7.9$ at 300 K (see Figures 5c and 7e in ref 30).

The steady-state coherence functions $C(n)$ calculated for the LH2 antenna with $M_{12} = 300$, 400, and 500 cm^{-1} are shown in Figure 5. The corresponding site inhomogeneity values are $\sigma = 340$, 450, and 550 cm^{-1}, respectively. The effective length of the exciton wavepacket can be estimated as $N_{coh} = 4.4$, 5.0, and 5.7. We recall that Kühn et al.[25] obtained $N_{coh} = 4$ in the steady-state limit for the same antenna complex at room temperature assuming $M_{12} = 300$ cm^{-1} and $\sigma = 700$ cm^{-1} (FWHM).

It should be pointed out that the localization sizes for the B850 antenna, $N_{eff} = 7.87$ and $N_{coh} = 5.0$, obtained here reflect an effective size of the exciton wavefunctions and their steady-state superposition. But they do not correspond to any physical size, i.e., the size of some fragment that can be removed from the antenna without significant changes of its spectral properties. For example, if we cut off the fragment containing five molecules (i.e., corresponding to the coherence size), we will destroy the coherence between molecules within and outside this effective coherence area (see Figure 5). Some kind of spectroscopic techniques may be very sensitive to these nonlocal interactions.[38] Figure 2 shows that we need a fragment of more than 12 molecules to explain the results of our relative difference absorption measurements (the difference absorption shapes of the antenna and the dimeric subunit as well as their relative amplitudes). So, our technique of relative difference absorption measurements reveals the spectroscopic subunit size of about 12 molecules. The same size was suggested by modeling of the CD spectra of the B850 antenna of *Rps. acidophila*.[11,38] In contrary, a much smaller spectroscopic subunit size was obtained by modeling the shape of the difference absorption of the B850 antenna of *Rb. sphaeroides*.[18] Pullerits et al.[18] demonstrated that a fragment of the B850 ring containing four molecules reproduced the experimental pump−probe profile. This is not in contradiction with our simulation, because we are also able to explain only the difference absorption shape using a subunit size of four molecules. Indeed, in Figure 2 we show that the shape of the difference absorption corresponding to $N = 4$ is not very different from those corresponding to $N = 12$ and $N = 18$. Some scaling and shifting of the $N = 4$ curve allow us to fit the experimental shape for the B850 antenna, i.e., to reproduce the result of ref 18. But we also have shown that for $N = 4$ it is impossible to explain the amplitude of the difference absorption for the antenna. We conclude that the difference absorption shape gives us only fragmentary information about exciton dynamics due to lack of information about the amplitude. The method of relative difference absorption measurements proposed here reveals a more complete picture, which allows us to obtain with high precision a variety of delocalization sizes, such as the effective sizes N_{eff}, N_{coh}, and the spectroscopic subunit size.

5. Discussion

We have performed a comparative study of the nonlinear spectral response of two different molecular aggregates: the peripheral light-harvesting complex, LH2, of the purple photosynthetic bacterium *Rb. sphaeroides* containing 18 light-harvesting B850 BChl molecules arranged in a ringlike structure and the elementary LH1 antenna subunit, B820, containing 2 BChls.

The B820 dimeric subunit is a good example of a small-size aggregate. Such aggregates have only a few exciton levels (N one-exciton and $N(N-1)/2$ two-exciton levels, where $N = 2$, 3, 4). The splitting between the levels is relatively large; i.e., larger than the line width, larger than the site inhomogeneity width, and larger than the room temperature thermal energy, k_BT. As a result the ESA and PB/SE components in the difference absorption spectrum do not overlap, and the amplitude of the difference absorption per absorbed photon, ΔA, is proportional to N. The exciton is almost completely delocalized over the small aggregate. The inverse participation ratio is close to the homogeneous limit for the quasi-linear aggregate: $N_{eff} = (2/3)(N + 1)$. This complete delocalization is not significantly influenced by the site inhomogeneity and does not depend on temperature (because even at room temperature only the lowest level is populated). So, in the small aggregate limit we have $\Delta A \sim N$, $N_{eff} \cong (2/3)(N + 1)$, and $N_{coh} \cong (2/3)(N + 1)$. In the case of a dimer ($N = 2$) we have $N_{eff} \cong 2$ and $N_{coh} \cong 2$. A complete delocalization implies that the spectral features of a small aggregate are determined by the cooperative behavior of all the molecules, so that the spectroscopic subunit size is also the same as the physical size of the system, N.

On the other hand, the B850 antenna of the LH2 complex corresponds to the large aggregate limit ($N >> 5$). For large aggregates there are many exciton levels with a relatively small

splitting between them. The splitting between the most intense one- and two-exciton transitions is much less than the corresponding line widths. The splitting between the one-exciton levels is several times smaller than the site inhomogeneity and the room temperature thermal energy. In this case the ESA and PB/SE components are strongly overlapping and their combined contributions give rise to a very slow increase of ΔA with N. The delocalization of the individual exciton states is significantly reduced due to site inhomogeneity. Superposition of these states at room temperature results in the formation of an exciton wavepacket with a further reduction of the coherence length. For the large aggregate limit we have $\Delta A \sim c_1 - c_2/N$, $N_{\mathrm{eff}} < {}^2/_3N$, and $N_{\mathrm{coh}} < N_{\mathrm{eff}}$. For example, for the B850 antenna we have obtained $N_{\mathrm{eff}} \approx N/2 \div N/3$ and $N_{\mathrm{coh}} \approx N/4$. The size of spectroscopic subunit is less than the physical size of the aggregate due to disorder but more than the effective length of the wavefunctions, N_{eff}. We estimate this size as $N/2 \div {}^2/_3N$.

Notice that the delocalization degree can be obtained from other techniques that give information about the dipole strength of the exciton levels. The superradiance measurements of the LH2 complex of *Rb. sphaeroides* showed that the emitting dipole strength of the lowest exciton level of the B850 band is equal to 2.8 (in the units of the monomeric dipole strength).[9] Nonlinear absorption measurements have revealed the giant absorption cross-section in the B850 band of the same complex.[22,23] The corresponding dipole strength was estimated as 16 ± 4 (in the units of the monomeric dipole strength).[22] According to our model the B850 absorption band is determined by 3−5 of the lowest exciton levels (the $k = 0, \pm 1$, and ± 2 levels). The dipole strengths of these levels are 2.41, 6.40, 6.52, 0.95, and 0.68 (in increasing order of energy). In the homogeneous limit we will have 0.03, 8.83, 8.83, 0.0, and 0.0. We conclude that the calculated dipole strength of the lowest level, i.e., 2.41, is in good agreement with the experimental value of 2.8 revealed by the superradiance data.[9] But the dipole strength of 16 suggested by Leupold and co-workers[22] is difficult to interpret, because the upper limit for a circular aggregate of 18 BChls (with the in-plane orientation of transition dipoles) is equal to 9. For the disordered aggregate for our parameter set this value is 6−7.

In summary, we have obtained a consistent and quantitative fit of the pump−probe spectra of the dimeric subunit B820 and the LH2 (B850) antenna of *Rb. sphaeroides*. We estimate that the nearest-neighbors interaction energy in the antenna is about 400 cm^{-1} and the diagonal disorder is about 450 cm^{-1}. These values correspond to the effective delocalization length of the wavefunctions $N_{\mathrm{eff}} = 7.87$ and the coherence length of the room-temperature wavepacket $N_{\mathrm{coh}} = 5.0$. The amplitude of the difference absorption reflects a cooperative behavior within at least 12 BChls. We suggest that the dimeric subunit is characterized by a decrease of the interaction energy to 300 cm^{-1} together with an increase of the disorder value to 600 cm^{-1}.

The next step in understanding the origins of the nonlinear response of photosynthetic antenna requires the consideration of both static and dynamic disorder (strong exciton−phonon coupling). Strong coupling may give rise to further reduction of the disorder-induced localization length due to polaron formation.[32−35] In this case the amplitude of nonlinear response will be determined by a combined action of the static and dynamic disorder. To describe the experimental ratio of amplitudes we most probably will need smaller values of the static disorder together with non-zero values of the dynamic disorder. At this moment we restrict ourselves to a more simple picture, where the combined action of all localization factors is modeled by some effective value of the static diagonal disorder. At this level of approximation we do not study the dynamic aspects of localization and analyze only the steady-state values.

Acknowledgment. V.N. was supported by a visitor's grant from the Dutch Foundation of Scientific Research (NWO) and by the Russian Foundation for Basic Research, Grant No. 99-04-49217. We acknowledge the help of Marion Van Brederode in performing the pump−probe experiments. The research was supported by the Foundation of Earth and Life Sciences (ALW), part of the Dutch Foundation of Scientific Research and the Human Frontiers in Science Program, Grant No. 1932802.

References and Notes

(1) Van Grondelle, R.; Dekker, J. P.; Gillbro, T.; Sundström, V. *Biochim. Biophys. Acta* **1994**, *1187*, 1.
(2) Zuber, H.; Cogdell, R. J. In *Anoxygenic Photosynthetic Bacteria*; Blankenship, R. E., Madigan, M. T., Bauer, C. E., Eds.; Kluwer Academic Publishers: Dordrecht/Boston/London, 1995.
(3) McDermott, G.; Prince, S. M.; Freer, A. A.; Hawthornthwaite-Lawless, A. M.; Papiz, M. Z.; Cogdell, R. J.; Isaacs, N. W. *Nature* **1995**, *374*, 517.
(4) Koepke, J.; Hu, X.; Muenke, C.; Schulten, K.; Michel, H. *Structure* **1996**, *4*, 581.
(5) Karrasch, S.; Bullough, P. A.; Ghosh, R. *EMBO J.* **1995**, *14*, 631.
(6) Jimenez, R.; Dikshit, S. N.; Bradforth, S. E.; Fleming, G. R. *J. Phys. Chem.* **1996**, *100*, 6825.
(7) Sauer, K.; Cogdell, R. J.; Prince, S. M.; Freer, A.; Isaacs, N. W.; Sheer, H. *Photochem. Photobiol.* **1996**, *64*, 564.
(8) Alden, R. G.; Johnson, E.; Nagarajan, V.; Parson, W. W.; Law, C. J.; Cogdell, R. J. *J. Phys. Chem. B* **1997**, *101*, 4667.
(9) Monshouwer, R.; Abrahamsson, M.; van Mourik, F.; van Grondelle, R. *J. Phys. Chem. B* **1997**, *101*, 7241.
(10) Hu, X.; Ritz, T.; Damjanovic, A.; Schulten, K. *J. Phys. Chem. B* **1997**, *101*, 3854.
(11) Koolhaas, M. H. C.; van der Zwan, G.; Frese, R. N.; van Grondelle, R. *J. Phys. Chem. B* **1997**, *101*, 7262.
(12) Koolhaas, M. H. C.; Frese, R. N.; Fowler, G. J. S.; Bibby, T. S.; Georgakopoulou, S.; van der Zwan, G.; Hunter, C. N.; van Grondelle, R. *Biochemistry* **1998**, *37*, 4693.
(13) Liuolia, V.; Valkunas, L.; van Grondelle, R. *J. Phys. Chem. B* **1997**, *101*, 7343.
(14) Wu, H.-M.; Reddy, N. R. S.; Small, G. J. *J. Phys. Chem. B* **1997**, *101*, 651.
(15) Wu, H.-M.; Ratsep, M.; Lee, I.-J.; Cogdell, R. J.; Small, G. J. *J. Phys. Chem. B* **1997**, *101*, 7654.
(16) Scholes, G. D.; Gould, I. R.; Cogdell, R. J.; Fleming, G. R. *J. Phys. Chem. B* **1999**, *103*, 2543.
(17) Novoderezhkin, V. I.; Monshouwer, R.; van Grondelle, R. *Biophys. J.* **1999**, *77*, 666.
(18) Pullerits, T.; Chachisvilis, M.; Sundström, V. *J. Phys. Chem.* **1996**, *100*, 10787.
(19) Kennis, J. T. M.; Streltsov, A. M.; Aartsma, T. J.; Nozava, T.; Amesz, J. *J. Chem. Phys.* **1996**, *100*, 2438.
(20) Novoderezhkin, V. I.; Taisova, A. S.; Fetisova, Z. G.; Blankenship, R. E.; Savikhin, S.; Buck, D. R.; Struve, W. S. *Biophys. J.* **1998**, *74*, 2069.
(21) Novoderezhkin, V. I.; Fetisova, Z. G. *Biophys. J.*, in press.
(22) Leupold, D.; Stiel, H.; Teuchner, K.; Nowak, F.; Sandner, W.; Ücker, B.; Scheer, H. *Phys. Rev. Lett.* **1996**, *77*, 4675.
(23) Leupold, D.; Stiel, H.; Ehlert, J.; Nowak, F.; Teuchner, K.; Voigt, B.; Bandilla, M.; Ücker, B.; Scheer, H. *Chem. Phys. Lett.* **1999**, *301*, 537.
(24) Chachisvilis, M.; Kühn, O.; Pullerits, T.; Sundström, V. *J. Phys. Chem. B* **1997**, *101*, 7275.
(25) Kühn, O.; Sundström, V. *J. Chem. Phys.* **1997**, *107*, 4154.
(26) Bradforth, S. E.; Jimenez, R.; van Mourik, F.; van Grondelle, R.; Fleming, G. R. *J. Phys. Chem.* **1995**, *99*, 16179.
(27) Jimenez, R.; van Mourik, F.; Yu, J. Y.; Fleming, G. R. *J. Phys. Chem. B* **1997**, *101*, 7350.
(28) Monshouwer, R., Baltuška, A.; van Mourik, F.; van Grondelle, R. *J. Phys. Chem. A* **1998**, *102*, 4360.
(29) Nagarajan, V.; Johnson, E. T.; Williams, J. C.; Parson, W. W. *J. Phys. Chem. B* **1999**, *103*, 2297.
(30) Meier, T.; Chernyak, V.; Mukamel, S. *J. Phys. Chem. B* **1997**, *101*, 7332.
(31) Kühn, O.; Mukamel, S. *J. Phys. Chem. B* **1997**, *101*, 809.
(32) Meier, T.; Zhao, Y.; Chernyak, V.; Mukamel, S. *J. Chem. Phys.* **1997**, *107*, 3876.

(33) Meier, T.; Chernyak, V.; Mukamel, S. *J. Chem. Phys.* **1997**, *107*, 8759.

(34) Zhang, W. M.; Meier, T.; Chernyak, V.; Mukamel, S. *J. Chem. Phys.* **1998**, *108*, 7763.

(35) Zhang, W. M.; Meier, T.; Chernyak, V.; Mukamel, S. *Phil. Trans. R. Soc. London A* **1998**, *356*, 405.

(36) Fidder, H.; Knoester, J.; Wiersma, D. A. *J. Chem. Phys.* **1991**, *95*, 7880.

(37) Mukamel, S. *Principles of nonlinear optical spectroscopy*; Oxford University Press: New York, 1995.

(38) Koolhaas, M. H. C.; van der Zwan, G.; van Grondelle, R. *J. Phys. Chem. B*, submitted.

(39) Kennis, J. T. M.; Aartsma, T. J.; Amesz, J. *Biochim. Biophys. Acta* **1994**, *1188*, 278.

(40) Xiao, W.; Lin, S.; Taguchi, A. K. W.; Woodbury, N. W. *Biochemistry* **1994**, *33*, 8313.

(41) Monshouwer, R. The nature and dynamics of excitations in photosynthetic light-harvesting. Ph.D. thesis, Vrije Universiteit Amsterdam, 1998.

(42) Visser, H. M.; Somsen, O. J. G.; van Mourik, F.; Lin, S.; van Stokkum, I. H. M.; van Grondelle, R. *Biophys. J.* **1995**, *69*, 1083.

(43) Loach, P. A.; Parkes, P. S.; Miller, J. F.; Hinchigeri, S. B.; Callahan, P. M. In *Cold Spring Harbor Symposium on Molecular Biology of the Photosynthetic Apparatus*; Arntzen, C., Bogorad, L., Bonitz, S., Steinback, K., Eds.; Cold Spring Harbor Laboratory: Cold Spring Harbor, 1985.

(44) Chang, M. C.; Callahan, P. M.; Parkes-Loach, P. S.; Cotton, T. M.; Loach, P. A. *Biochemistry* **1990**, *29*, 421.

(45) Visschers, R. W.; Chang, M. C.; van Mourik, F.; Parkes-Loach, P. S.; Heller, B. A.; Loach, P. A.; Van Grondelle, R. *Biochemistry* **1991**, *30*, 5734.

(46) Van Mourik, F.; van der Oord, C. R. J.; Visscher, K. J.; Parkes-Loach, P. S.; Loach, P. A.; Visschers, R. W.; van Grondelle, R. *Biochim. Biophys. Acta* **1991**, *1059*, 111.

(47) Koolhaas, M. H. C.; van Mourik, F.; van der Zwan, G.; van Grondelle, R. *J. Luminesc.* **1994**, *60,61*, 515.

(48) Koolhaas, M. H. C.; van der Zwan, G.; van Mourik, F.; van Grondelle, R. *Biophys. J.* **1997**, *72*, 1828.

(49) Davydov, A. S. *Theory of molecular excitons*; Plenum Press: New York, 1971.

(50) Juzeliunas, G. *Z. Phys. D* **1988**, *8*, 379.

(51) Van Burgel, M.; Wiersma, D. A.; Duppen, K. *J. Chem. Phys.* **1995**, *102*, 20.

(52) Kennis, J. T. M. *Exciton coupling, energy transfer and photochemical conversion in purple photosynthetic bacteria.* Ph.D. thesis, Rijksuniversiteit Leiden, 1997.

(53) Van Mourik, F. *Spectral inhomogeneity of the bacterial light-harvesting antennae: causes and consequences.* Ph.D. thesis, Vrije Universiteit Amsterdam, 1993.

(54) Beekman, L. M. P.; Steffen, M.; van Stokkum, I. H. M.; Olsen, J. D.; Hunter, C. N.; Boxer, S. J.; van Grondelle, R. *J. Phys. Chem. B* **1997**, *101*, 7284.

(55) Somsen, O. J. G.; Chernyak, V.; Frese, R. N.; van Grondelle, R.; Mukamel, S. *J. Phys. Chem. B* **1998**, *102*, 9577.